ACS OMEGA

http://pubs.acs.org/journal/acsodf

Article

Acrylamide: New Organic Solvent with Chemically Tunable Viscosity for Rapid Gram-Scale Synthesis of Gold Nanoparticles

Yoon Hyuck Kim and Jae-Seung Lee*

Cite This: *ACS Omega* 2022, 7, 45277−45286

Read Online

ACCESS | Metrics & More | Article Recommendations | Supporting Information

ABSTRACT: Noble metal nanoparticles have demonstrated various biomedical, optical, and electronic applications owing to their unique chemical and physical properties. However, their gram-scale synthesis remains a challenge. We have developed a method for the gram-scale synthesis of gold nanoparticles (AuNPs) using acrylamide (AAm) as a solvent. AAm possesses unique properties such as low melting temperature, high solvating power, and high solubility of its polymer (polyacrylamide(pAAm)) in water. The viscosity of the AAm solvent can be chemically tuned by the polymerization of AAm and addition of a low-volatile diluent, which can stabilize highly concentrated as-synthesized AuNPs in gram quantities. The synthesized AuNPs are substantially stable and catalytically active under high ionic strength conditions owing to the pAAm protection on the particle surface. Further, the synthesis mechanism of the AuNPs has been thoroughly investigated. The versatility of the synthesis method is proved by synthesizing other mono-(Ag and Pd) and bimetallic (Au + Pd and Ag + Pd) nanoparticles using the AAm solvent with controlled viscosity. Importantly, the productivity of this synthetic strategy is the highest among the previously reported gram-scale synthesis methods of AuNPs. To the best of our knowledge, our study presents the use of acrylic monomer as a solvent for the gram-scale synthesis of noble metal nanoparticles for the first time. This study significantly extends the list of solvents with chemically tunable viscosity by including other acrylic reagents for nanomaterial synthesis, functionalization, and catalytic, optical, and electrical reactions under highly localized reaction conditions.

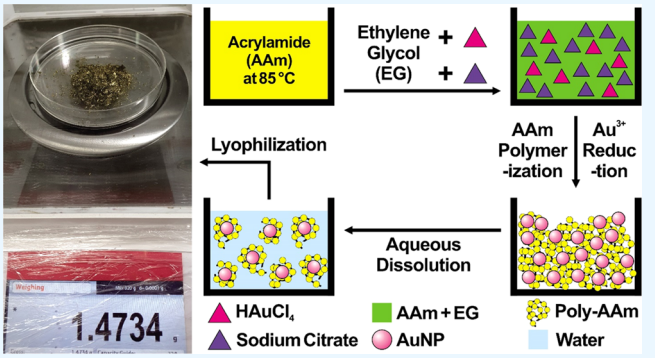

INTRODUCTION

Solution-phase gram-scale synthesis of noble metal nanoparticles is crucial in transferring bench-top experiments conducted on a micro- or milliliter scale to practical and industrial applications.[1−10] However, the productivity (a measure of synthesis efficiency in terms of reaction volume and time as well as the mass of the final product) of nanoparticle synthesis in the solution phase is often low. The limited productivity in batch synthesis is mainly due to (1) the production of nanoparticles with undesired shapes and sizes, owing to the increase in reaction volume and consequent changes in the nucleation and growth kinetics, and (2) instability of nanoparticles when produced at high concentrations. Particularly, nanoparticles cannot electrostatically repel each other at high concentrations and inevitably come into contact owing to Brownian motion, resulting in irreversible aggregation. In addition to electrostatic forces, the steric forces cause particle stabilization according to the extended Derjaguin−Landau−Verwey−Overbeek (DLVO) theory. In most cases, the theory explains nanoparticle stabilization using polymeric materials such as poly(ethylene glycol) or poly(vinyl pyrrolidone) as physical barriers on the nanoparticle surface.[11] For protection and surface modification, the synthesis of noble metal nanoparticles with various surface ligands has been developed in a variety of methods.[1,10,12−16] Organic solvents are typically preferred to maximize steric stabilization because they allow the protecting agents to densely adhere to the nanoparticle surface owing to their low polarity. For gram-scale synthesis, however, developing new synthesis media possessing ideal properties is necessary. First, the media initially must possess low viscosity, preferably almost liquid-like properties, for the homogeneity of the reaction mixtures at the beginning of the synthesis. Second, the media should exhibit high solvating power to dissolve the reactants, even at high concentrations. Third, as the nucleation and growth of the nanoparticles occur, the media are expected to become far more viscous, almost solid-like, owing to the increased steric stability of the nanoparticles. Lastly, the media should be easily removable to obtain only nanoparticles as a product.

Received: September 7, 2022
Accepted: November 21, 2022
Published: December 2, 2022

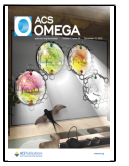

https://doi.org/10.1021/acsomega.2c05813
ACS Omega 2022, 7, 45277−45286

Acrylamide (AAm) is a polar unsaturated amide. Its molecular weight (71.08 g/mol) is as low as those of common organic solvents such as butanol (74.12 g/mol), dimethylformamide (73.09 g/mol), dimethyl sulfoxide (78.13 g/mol), hexane (86.18 g/mol), and benzene (78.11 g/mol); however, AAm exists as a solid material at room temperature owing to its high polarity. Although AAm is readily soluble in water and polar organic solvents, it is also partly hydrophobic owing to its vinyl group, which allows it to polymerize when chemically triggered. Currently, AAm is best known as a precursor to polyacrylamides (pAAms) that are used in various academic and industrial applications, such as pAAm gel for electrophoresis and flocculation agents for water purification.[17,18] In nanoparticle synthesis, pAAm protects the nanoparticles as surface ligands or forms a bulk hydrogel matrix to immobilize the synthesized nanoparticles.[19,20] Based on its unique chemical and physical properties, we hypothesize that liquified AAm (heated above its melting temperature (84.5 °C)) could be a versatile organic solvent with high solvating power. Importantly, employing liquified AAm in nanoparticle synthesis has never been attempted. The AAm solvent can polymerize to innately increase its viscosity during nanoparticle synthesis, preventing the collision of nanoparticles to decrease the probability of their irreversible aggregation. Moreover, the resultant pAAm is readily soluble in water, allowing efficient removal. Considering the four conditions required for the gram-scale synthesis of nanoparticles mentioned above, AAm could be a suitable medium because its polymerizability is chemically controlled.

Herein, we present an AAm solvent for gram-scale, one-pot synthesis of gold nanoparticles (AuNPs). The viscosity of the designed solvent is easily controlled by polymerization and diluent addition, which is attractive for stabilizing highly concentrated AuNPs during and after synthesis. Moreover, this strategy is highly versatile and can be applied to synthesize other types of noble metal nanoparticles.

EXPERIMENTAL SECTION

Materials and Instrumentation. Acrylamide (AAm; Cat.# A9099), ethylene glycol (EG; Cat.# 102466), sodium citrate tribasic (SC; Cat.# S4641), gold(III) chloride trihydrate ($HAuCl_4 \cdot 3H_2O$; Cat.# 520918), palladium(II) nitrate dihydrate (Cat.# 76070), silver nitrate ($AgNO_3$; Cat.# 204390), 11-mercaptoundecanoic acid (MUA; Cat.# 450561), sodium chloride (NaCl; Cat.# S76070), dihydroethidium (DHE; Cat.# D7008), propionamide ($CH_3CH_2CONH_2$; Cat.# 143936), tris-EDTA buffer solution (pH 8.0, [Tris-HCl] = 1 M, [EDTA] = 0.1 M; Cat.# T9285), 4-nitrophenol (99%, Cat.# 241326), and sodium borohydride ($NaBH_4$; Cat.# C1629) were purchased from Sigma-Aldrich (St. Louis, MO). Phosphate buffer saline (PBS; 10×, pH 6.8; Cat.# LB201-02) and minimum essential medium (MEM; 1×; Cat.# LM007-54) were purchased from Welgene Inc. (Gyeongsan-si, Republic of Korea). For every experiment, ultrapure water was supplied by a Direct-Q3 system (Millipore, Billerica, MA). For the analysis of the synthesized nanoparticles and their synthesis reactions, a Talos F200X transmission electron microscope (Thermo Fisher Scientific Inc., Waltham, MA), Tecnai G^2 F30 scanning electron microscope (Field Electron and Ion Company, Hillsboro, OR), Zetasizer Nano ZS90 size and ζ-potential analyzer (Malvern Panalytical, Malvern, UK), Cary100 ultraviolet−visible (UV−vis) spectrophotometer (Agilent Technologies, Santa Clara, CA), Cary Eclipse fluorescence spectrophotometer (Agilent Technologies, Santa Clara, CA), Cary 630 Fourier transform infrared spectrometer (Agilent Technologies; Santa Clara, CA), 1260 Infinity II LC System analytical high-performance liquid chromatography (HPLC) system (Agilent Technologies, Santa Clara, CA), and FD8508 freeze-dryer (ilShinBioBase Co., Yangju-si, Republic of Korea) were used.

Synthesis of AuNPs in AAm Solvent. In a typical experiment, AAm (50 mmol, 3.554 g) was liquified at 85 °C for use as the solvent. To control the viscosity of the final solution, EG was combined with AAm as a low-volatile diluent at mole ratios of EG and AAm ranging from 0:5 to 5:0 (0:5, 1:4, 2:3, 3:2, 4:1, 5:0; 50 mmol in total). Subsequently, $HAuCl_4$ (25 μmol, 0.0098 g; 1× $HAuCl_4$) and SC (3.5 mmol, 1.029 g; 1× SC) were dissolved in the solvent, giving a yellow solution. The solution was heated manually using a glass rod. As the synthesis proceeded, the viscosity of the solution gradually increased; the color of the solution changed from yellow to red, indicating the synthesis of AuNPs along with the polymerization of AAm. After the color stopped changing, the viscous solution was cooled to room temperature, combined with water, and placed on a shaker to dissolve pAAm and the pAAm-capped AuNPs (pAAm-AuNPs). The AuNPs were washed via centrifugation (13,000 rpm, 20 min), and the supernatant was removed. The AuNPs were then redispersed in water. The washing process was repeated thrice.

Detection of Radicals Using DHE. DHE solution (300 μL, 2 mM) was added to four combinations of aqueous solutions (2.7 mL): (1) water (blank), (2) $HAuCl_4$, (3) $HAuCl_4$ and propionamide, and (4) $HAuCl_4$ and AAm. The final molar concentration of DHE is 200 μM, $HAuCl_4$ 1 mM, propionamide 500 mM, and AAm 500 mM. The photoluminescence (PL) spectra were obtained using a Cary Eclipse fluorescence spectrophotometer (excitation wavelength = 515 nm).

Molecular Weight Analysis of pAAm Using Gel Permeation Chromatography (GPC). pAAm was obtained from the supernatant collected after the first centrifugation of the dissolved pAAm-AuNPs. After the supernatant was filtered using 0.45 μm nylon filters to remove any solid impurities, the aqueous pAAm was buffered to pH 7. The GPC data for pAAm were obtained using an analytical HPLC system (1260 Infinity II LC System) at a rate of 1 mL/min at 40 °C.

Synthesis of Ag, Pd, Au + Pd, and Ag + Pd Nanoparticles in AAm Solvent. The synthesis of mono- (Ag and Pd) and bimetallic (Au + Pd and Ag + Pd) nanoparticles was similar to that of pAAm-AuNPs. EG (30 mmol, 1.802 g) and SC (3.5 mmol, 1.029 g) were dissolved in AAm (20 mmol, 1.422 g) at 85 °C. The types and combinations of metal precursors investigated in this study are listed in Table S1 (Supporting Information). Subsequently, the metal precursors were dissolved in the solution, which was heated while stirring using a glass rod. The viscosity of the heated solutions gradually increased, and color changes were observed in each solution, as shown in Table S1 (Supporting Information). After the color change, the resultant mixtures were cooled to 25 °C. The mixtures were then dissolved in water (30 mL) to obtain nanoparticles. The nanoparticles were washed by centrifugation (13,000 rpm, 20 min), and the supernatant was removed. The nanoparticles were then redispersed in water. The washing process was repeated thrice.

Synthesis of Citrate-Capped AuNPs (SC-AuNPs). SC-AuNPs were synthesized based on the Turkevich−Frens

https://doi.org/10.1021/acsomega.2c05813
ACS Omega 2022, 7, 45277−45286

method.[21] First, 49 mL of water was boiled in an Erlenmeyer flask. The $HAuCl_4$ (1 mL, 12.7 mM) and SC (0.94 mL, 38.8 mM) solutions were then rapidly injected into boiling water with stirring. After 5 min, the color of the aqueous solution changed from yellow to red, indicating the successful SC-AuNP synthesis. The SC-AuNP solution was cooled to 25 °C. Pure SC-AuNPs were obtained by centrifugation at 13,000 rpm for 20 min, supernatant removal, and redispersion in water. This process was repeated thrice.

MUA-Functionalization of SC-AuNPs and pAAm-AuNPs. MUA was added to each of the SC-AuNP and pAAm-AuNP solutions buffered with tris-EDTA buffer (pH 8.0, [Tris-HCl] = 100 mM, [EDTA] = 10 mM, [MUA] = 0.5 mM, and [AuNP] = 1 nM each). After incubation for 2 h at 25 °C, tris-HCl, EDTA, and unreacted MUA were removed by centrifugation (13,000 rpm, 20 min). The supernatant was removed, and the AuNPs were redispersed in water. The washing process was repeated thrice.

Catalytic Reaction Using the SC-AuNPs and pAAm-AuNPs. A 4-nitrophenol solution (100 μL, 4 mM) and a $NaBH_4$ solution (500 μL, 80 mM) were mixed with water (300 μL). To this mixture solution, either the SC- or pAAm-AuNP solution (100 μL, 1 nM) was injected. After 15 min, the solution was centrifuged to spin down the AuNPs (13,000 rpm, 15 min). The absorbance of the supernatant was measured using UV−vis spectroscopy. The AuNPs were collected and mixed with freshly prepared 4-nitrophenol and $NaBH_4$ mixture solutions for another catalytic reaction. The entire catalytic reaction procedure was repeated five times.

Gram-Scale Synthesis of pAAm-AuNPs Using AAm Solvent. The gram-scale synthesis of AuNPs was similar to the regular-scale synthesis of AuNPs (see above). AAm (635.2 mmol, 45.15 g) was liquified at 85 °C in a 1 L glass beaker for use as a solvent. EG (952.8 mmol, 57.23 g), SC (11.12 mmol, 3.27 g), and $HAuCl_4$ (7.94 mmol as in $HAuCl_4{\cdot}3H_2O$, 3.127 g) were dissolved in the solvent using a glass rod. The final volume of the reaction mixture was ∼100 mL. The solution was heated manually while stirring with a glass rod. After the synthesis was completed, the produced AuNPs were collected in an aqueous solution using the methods used for the regular-scale synthesis of AuNPs, including water dissolution and centrifugation. Finally, the AuNPs were obtained as a dry powder via lyophilization.

RESULTS AND DISCUSSION

AAm was used as a solvent because of its polymerizable property and low melting temperature (84.5 °C). At the beginning of the synthesis (Scheme 1), solid AAm is liquified at 85 °C (Figure 1a), to which sodium citrate (SC) and $HAuCl_4$ were added and dissolved. After 5 min, its color turned dark red, indicating AuNP synthesis. The consequent color change is due to the localized surface plasmon resonance (LSPR) in the AuNPs. Meanwhile, the viscosity of the solution gradually increased owing to the polymerization of AAm into polyacrylamide (pAAm). Although pAAm is known to be soluble in water, the dissolution of the resultant AuNP-embedded pAAm solid mixture in water was limited even after several days of stirring, probably because of the highly complex entanglement of the pAAm chains. To dissolve the AuNP-embedded pAAm solid block in water, we prepared a series of synthetic mixtures composed of the same reagents and added ethylene glycol (EG) at different mole ratios with AAm. EG acts as a low-volatile diluent that neither vaporizes at higher

Scheme 1. Schematic of the Gold Nanoparticle (AuNP) Synthesis Using an Acrylamide (AAm) Solvent[a]

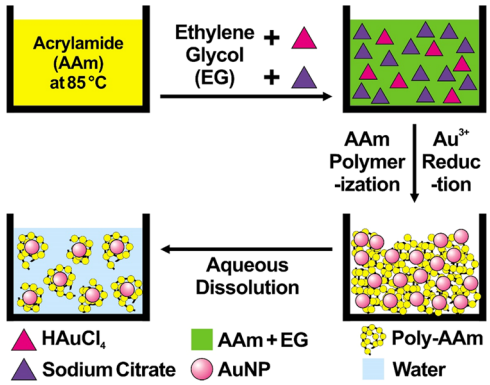

[a]The three precursors (EG, SC, and $HAuCl_4$) are dissolved in the AAm solvent at 85 °C. As the reaction proceeds, Au^{3+} is reduced to the AuNPs during the polymerization of AAm. The AuNPs are collected by centrifugation after the AuNP-embedded pAAm composite is dissolved in water.

temperatures nor participates in the polymerization of AAm. EG was expected to decrease the degree of polymerization, leading to the enhanced water solubility of the resultant pAAm.[22] The mole ratio of EG to AAm was adjusted from 0:5 to 5:0 (50 mmol in total). As shown in Figure 1b, the products became less viscous as the amount of EG increased. In the absence of AAm (EG/AAm = 5:0), the product exhibited increased scattering, indicating the formation of large Au particle aggregates. This result implied that AAm is essential for stabilizing the AuNPs. To investigate the LSPR properties of the synthesized AuNPs as a function of the mole ratio of EG to AAm, we obtained and analyzed the UV−vis spectra of the AuNPs (Figure 1c,d). Interestingly, the wavelength at which the maximum extinction is observed (λ_{max}) remained almost the same at 524 nm, indicating that the size of the AuNPs was almost the same regardless of the mole ratio of EG to AAm, except EG/AAm = 5:0. However, unlike λ_{max}, the extinction of AuNPs at λ_{max} gradually increases as the EG mole ratio increases until EG/AAm = 3:2. When the proportion of EG is too large (EG/AAm = 4:1 and 5:0), the extinction of the AuNPs decreases, probably owing to insufficient protection of the AuNPs by either too short AAm or no AAm. The resulting uniformity of the spherical AuNPs, regardless of the mole ratio of EG and AAm, was further confirmed using transmission electron microscopy (TEM) (Figures 1e and S1, Supporting Information).

We analyzed the detailed synthesis mechanism of the AuNPs during AAm polymerization. Considering that the polymerization was initiated even without any added initiator, we expected that certain radical species would be generated by the reaction of $HAuCl_4$ and AAm. We monitored their generation during the reaction using DHE. DHE is oxidized by radical species to luminesce 2-hydroxyethidium, whose photoluminescence (PL) can be measured to quantify the radical species. We first characterized the PL of the mixture consisting of DHE, $HAuCl_4$, and AAm. The mixture exhibited strong emission at 620 nm (Figure 2a). This optical observation indicates that the polymerization of AAm was most likely initiated by the radical species generated by the reaction of $HAuCl_4$ and AAm. In contrast, $HAuCl_4$ without AAm did not result in any noticeable increase in the PL. Moreover, the

https://doi.org/10.1021/acsomega.2c05813
ACS Omega 2022, 7, 45277−45286

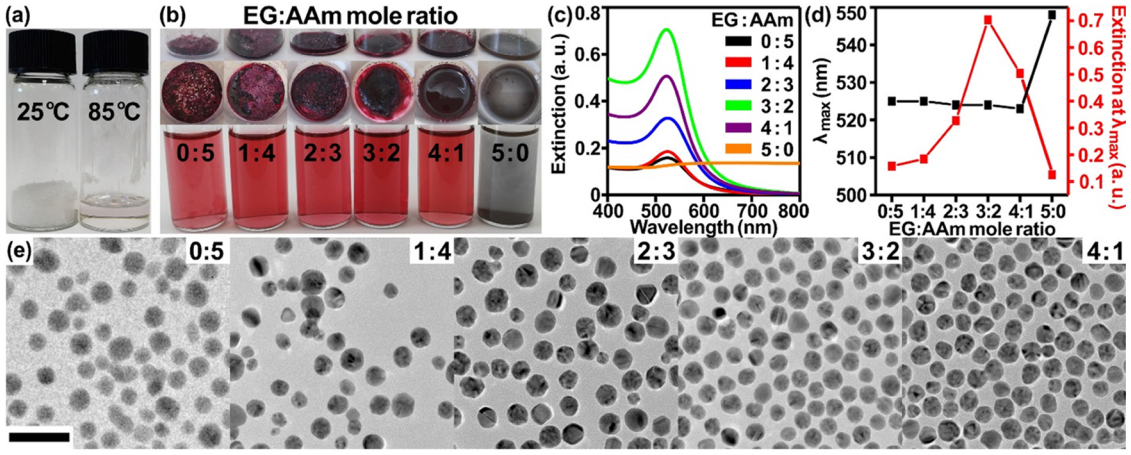

Figure 1. (a) Photograph showing AAm at 25 and 85 °C. (b) Photographs showing side and top views of the resultant product mixtures composed of ethylene glycol (EG) and AAm with mole ratios from 0:5 to 5:0 (50 mmol in total) and a photograph of the solutions containing the AuNPs obtained from each reaction batch. (c) UV−vis spectra of the AuNPs obtained from each reaction batch. (d) Plots showing the wavelength at which the maximum extinction was observed (λ_{max}) (black) and the extinction at λ_{max} (red) of the AuNPs. (e) Transmission electron microscopy (TEM) images of the AuNPs synthesized in the mixtures whose mole ratios of EG and AAm were 0:5, 1:4, 2:3, 3:2, and 4:1. The scale bar is 50 nm.

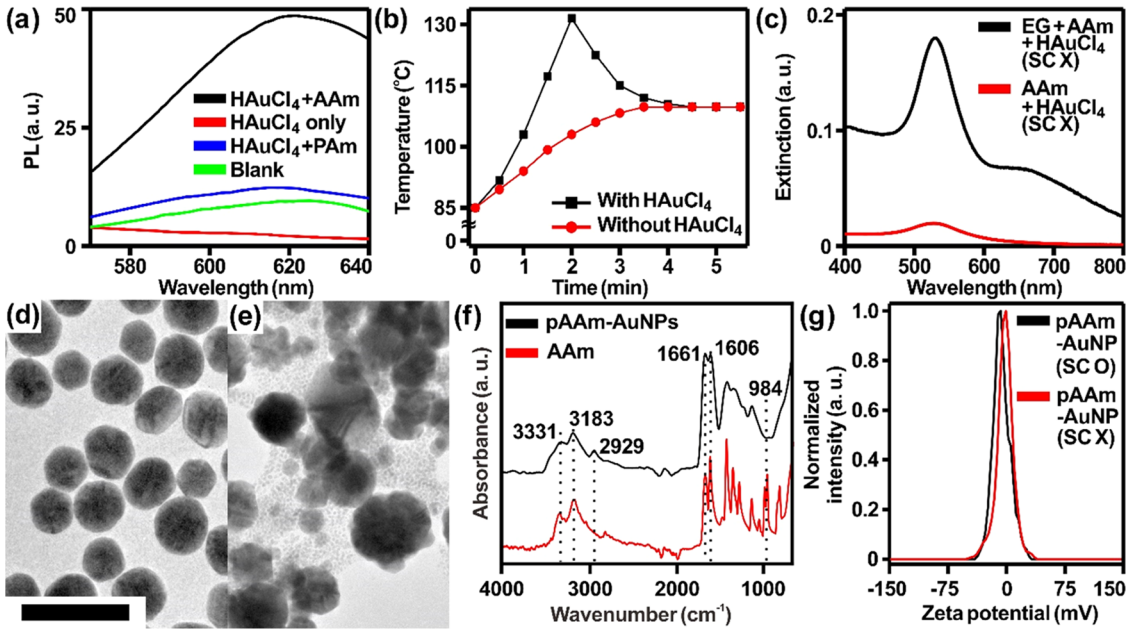

Figure 2. (a) Photoluminescence (PL) spectra of 2-hydroxyethidium that results from the reaction of dihydroethidium (DHE) with $HAuCl_4$ and AAm. $HAuCl_4$ and propionamide (PAm), $HAuCl_4$ only, and water (Blank) were also evaluated as controls. (b) Temperature profiles of the mixtures composed of EG, AAm, and SC with or without $HAuCl_4$ were obtained as a function of the reaction time. (c) UV−vis spectra of the AuNPs synthesized without SC in an AAm solution or an EG and AAm mixture solution (EG/AAm = 3:2). TEM images of the AuNPs synthesized in the mixtures composed of AAm and $HAuCl_4$ in the (d) presence and (e) absence of EG. The scale bar is 100 nm. (f) FT-IR spectra of the pAAm-AuNPs (EG/AAm = 3:2; 50 mmol in total) and AAm monomer show the presence of pAAm on the AuNP surface. (g) ζ-potential measurement of the AuNPs synthesized in the mixtures composed of EG, AAm, and $HAuCl_4$ with or without SC (pAAm-AuNP (SC O) and pAAm-AuNP (SC X)).

combination of $HAuCl_4$ and propionamide, an analogue of AAm, except for the absence of C═C, did not increase the PL. This observation indicates that the C═C double bond of AAm is the key chemical structure for radical formation. Once the polymerization began, its propagation proceeded very rapidly, terminating the synthesis in 5 min. The polymerization is exothermic and can accelerate (Figure 2b).[23] We also investigated the role of SC as a reductant in the synthesis of AuNPs by conducting the synthesis in the absence of SC. The UV−vis spectrum of the AuNPs exhibited a distinct absorption plasmon band at 530 nm owing to the LSPR of the AuNPs, with a broad shoulder around 650 nm, indicating partial aggregation of the AuNPs (Figure 2c). This result indicates that AAm and EG, in addition to SC, could also be responsible for reducing Au^{3+}.[24] However, the consumption of AAm as a reductant, in combination with the absence of SC, led to insufficient protection of the AuNPs and, consequently, irreversible aggregation of AuNPs. The reduction of Au^{3+} occurred even without EG and SC; however, the final product was less soluble in water, as shown in Figure 1b (EG/AAm = 0:5 in the presence of SC), resulting in the recovery of only a limited amount of AuNPs. Optical analysis of the AuNPs was

https://doi.org/10.1021/acsomega.2c05813
ACS Omega 2022, 7, 45277−45286

further correlated with electron microscopy observations of the synthesized AuNPs. Even in the absence of SC, the AuNPs synthesized in the mixture containing EG are uniform (40 nm in diameter; Figure 2d), while those without EG are highly polydispersed (10−70 nm in diameter; Figure 2e). This difference in uniformity is probably due to the reduction mechanisms, which depend on the reduction power of the reductants. In the presence of both EG and AAm, relatively monodisperse AuNPs could be synthesized because the more reductive agent primarily causes rapid nucleation, and the other less reductive agent slowly grows them (Figure 2d). The principle of this synthesis has been similarly demonstrated in the synthesis of uniform silver nanoparticles (AgNPs).[25] When only AAm was used for the synthesis without EG and SC, however, nucleation occurred slowly and sporadically, resulting in highly polydisperse AuNPs (Figure 2e). These results demonstrate that pAAm (as a primary protecting ligand) stabilizes high concentrations of AuNPs (pAAm-capped AuNPs; pAAm-AuNPs), while SC plays a role as a co-ligand along with pAAm. To identify the existence of pAAm on the AuNP surface, we obtained the Fourier transform infrared (FT-IR) spectrum of the pAAm-AuNPs and compared it with that of AAm (Figure 2f). Both the FT-IR spectra of the pAAm-AuNPs and AAm show absorption bands attributed to the asymmetric and symmetric N−H stretching bands of NH_2 (3331 and 3183 cm^{-1}, respectively) and characteristic peaks assigned to C═O stretching (1661 cm^{-1}) and N−H bending (1606 cm^{-1}) of the amide group.[26] In contrast, an absorption band of vibration of H in C═C−H (984 cm^{-1}) of AAm is not observed with the pAAm-AuNPs that show an absorption band at 2929 cm^{-1} for the asymmetric stretching of C−H in $C-H_2$. The similarity and difference of the two FT-IR spectra indicate that a polymerized form of AAm (pAAm) exists on the surface of the AuNP.[27] Furthermore, the larger negative ζ-potential (−7.5 mV) of the pAAm-AuNPs synthesized with SC implies the presence of SC on the surface in comparison with that of the pAAm-AuNPs synthesized without SC (−0.1 mV) (Figure 2g).

To investigate the chemical role of EG as a diluent, we obtained gel permeation chromatograms of the generated polymers and investigated the correlation between the weight-average molecular weight (M_w) and the mole ratio of EG (Figure 3). Because the generated polymers were not completely dissolved in water when the mole ratios of EG to AAm were 0:5 and 1:4, only the polymers generated when the mole ratios of EG to AAm were 2:3, 3:2, and 4:1 were analyzed after the removal of the pAAm-AuNPs by centrifugation. The gel permeation chromatograms of the three types of polymers exhibited a bimodal distribution; the first band indicates polymers in an M_w range of 10^4−10^5 g mol^{-1}, and the second band around M_w ~2200 g mol^{-1} (Figure 3a). The presence of much smaller polymers is due to the partial chemical quenching by SC as a radical scavenger during polymerization.[28] We further analyzed the changes in M_ws in response to the proportion of EG (Figure 3b). Interestingly, the M_ws of both the first and second bands decreased as the mole ratio of EG increased, indicating that the polymerization of AAm was inhibited owing to dilution by EG.

To analyze the effect of the amount of $HAuCl_4$ on pAAm-AuNPs, we prepared $HAuCl_4$ in various amounts (0.1×, 1×, 10×, and 100×; 1× = 25 μmol), each combined with EG and AAm (EG/AAm = 3:2; 50 mmol in total) and SC (1× = 3.5 mmol), for AuNP synthesis. The optical properties of the

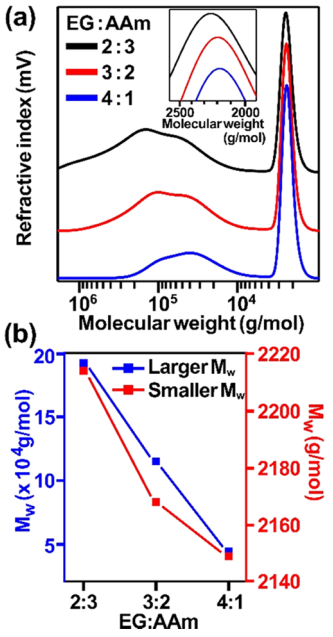

Figure 3. (a) Gel permeation chromatograms of pAAm obtained from the mixtures of EG and AAm with mole ratios 2:3, 3:2, and 4:1. (b) Plots showing the changes of the large and small M_w gel permeation chromatograms with varying EG-to-AAm mole ratios.

pAAm-AuNPs were analyzed using UV−vis spectroscopy (Figure 4a). When a large amount of $HAuCl_4$ was used (100×), a broad plasmon absorption band (λ_{max} = 555 nm) was observed owing to the scattering of large pAAm-AuNPs, in good agreement with the opaque brown color of the aqueous

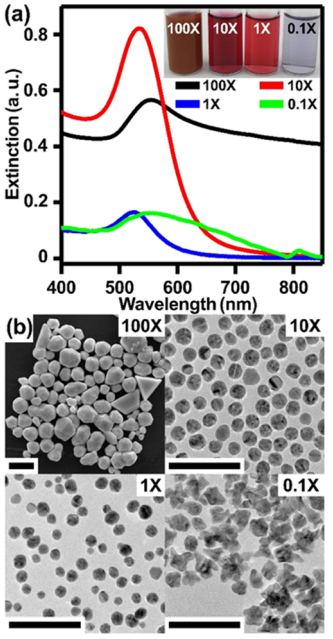

Figure 4. (a) UV−vis spectra of the pAAm-AuNPs as a function of the amount of $HAuCl_4$. (b) Scanning electron microscopy (SEM) image of the pAAm-AuNPs synthesized with 100× $HAuCl_4$ and TEM images of the pAAm-AuNPs synthesized with 10×, 1×, and 0.1× $HAuCl_4$ (1× = 25 μmol). The scale bars are 1 μm in the SEM image and 100 nm in the TEM images. The spectrum corresponding to 0.1× $HAuCl_4$ was 15 times as enhanced as the extinction of the original one.

https://doi.org/10.1021/acsomega.2c05813
ACS Omega 2022, 7, 45277−45286

solution (Figure 4a, inset). As the amount of $HAuCl_4$ decreased to 10× and 1×, strong LSPR properties of pAAm-AuNPs were observed, as evidenced by the distinctive plasmon absorption bands (λ_{max} = 534 and 524 nm for 10× and 1× $HAuCl_4$, respectively). Although the maximum extinctions were different owing to the different amounts of $HAuCl_4$, the spectral observations were in good agreement with the color of their aqueous solutions (Figure 4a, inset). However, when 0.1× $HAuCl_4$ was used, the UV−vis spectrum was broad, indicating nonuniform AuNPs. To understand the correlation between the optical and structural properties of the pAAm-AuNPs, we analyzed their morphology using scanning electron microscopy (SEM) and TEM. As shown in Figure 4b, the pAAm-AuNPs synthesized with 100× $HAuCl_4$ are several hundred nanometers in size, whereas those with 10× and 1× $HAuCl_4$ are 20 and 15 nm in diameter, respectively, suitable for exhibiting LSPR properties. In the nucleation-growth mechanism, the number of initially generated nuclei at 100× $HAuCl_4$ decreased as the mole ratio of SC to $HAuCl_4$ significantly decreased, essentially resulting in large pAAm-AuNPs.[29] At 0.1× $HAuCl_4$, however, nonuniform pAAm-AuNPs with irregular shapes were obtained, probably as a result of the dominance of kinetics over thermodynamics owing to the too-high reducing power of SC. Indeed, the mole ratio of SC to 0.1× $HAuCl_4$ increased 1000 times in comparison with its ratio to 100× $HAuCl_4$.[30]

To investigate the effect of the amount of SC on the morphology of pAAm-AuNPs, we prepared mixtures composed of EG, AAm, $HAuCl_4$, and SC for synthesizing pAAm-AuNPs. The amounts of EG, AAm, and $HAuCl_4$ were constant (EG/AAm = 3:2, 50 mmol in total; $HAuCl_4$ 10× = 250 μmol), but the amount of SC varied from 15× to 0× (1× = 3.5 mmol). We first analyzed the optical properties of the pAAm-AuNPs using UV−vis spectroscopy (Figure 5a). Distinct plasmon absorption bands were observed, whose broadness and λ_{max} increased as the amount of SC decreased, indicating a correlation between SC and the resultant pAAm-AuNPs. Specifically, as the amount of SC decreased from 15× to 0×, λ_{max} increased from 532 to approximately 650 nm, suggesting an overall increase in the diameter of the pAAm-AuNPs. The morphology of the pAAm-AuNPs was observed and analyzed using TEM (Figure 5b,c). As the amount of SC decreased from 15× to 1×, the pAAm-AuNPs became relatively uniform and slightly increased from 17 to 25 nm. Based on the nucleation-growth mechanism, this increase in AuNP diameter is attributed to the decreased number of nuclei at the initial stage of synthesis owing to the decreased reducing power.[29] Eventually, the diameter of the pAAm-AuNPs significantly increased to ∼90 nm on average in the absence of SC (0×). Moreover, the slow and progressive nucleation due to the absence of reductive SC resulted in a mixture of nonuniform AuNPs.

In addition to AuNPs, we investigated the versatility of this synthetic system for other noble metals, such as Ag, Pd, Au + Pd, and Ag + Pd. As expected, the AgNPs, palladium nanoparticles (PdNPs), and Au + Pd and Ag + Pd bimetallic nanoparticles (Au + PdNPs and Ag + PdNPs) were easily synthesized under representative synthetic conditions (EG/AAm = 3:2, 50 mmol in total; 1× SC; 0.2× Ag, 0.2× Pd, 0.5× Au + 0.5× Pd, or 0.5× Ag + 0.5× Pd) using $AgNO_3$, $Pd(NO_3)_2$, and $HAuCl_4$ as metallic precursors. The colors of the AgNP, PdNP, Au+PdNP, and Ag + PdNP solutions were yellow, dark gray, gray, and brown, respectively, owing to

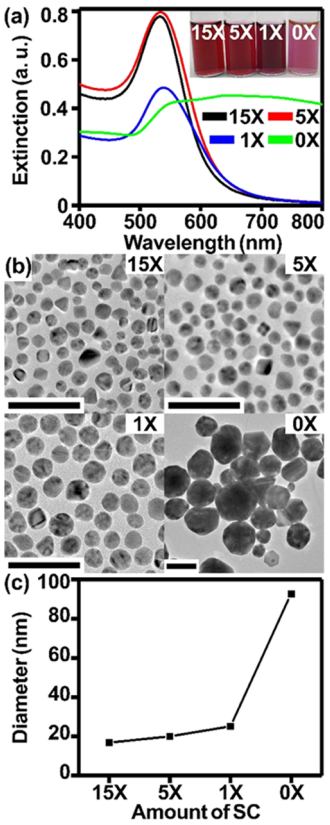

Figure 5. (a) UV−vis spectra and (b) TEM images of the pAAm-AuNPs synthesized with 15×, 5×, 1×, and 0× SC (1× = 3.5 mmol). All scale bars are 100 nm. (c) Plot showing the diameter of the pAAm-AuNPs as a function of the amount of SC. Except for the amount of SC, the synthetic conditions were the same as those of the mixtures shown in Figure 4, in which the amount of $HAuCl_4$ was 10×.

LSPR (mostly of AgNPs) and scattering. UV−vis spectra of AgNPs, PdNPs, Au + PdNPs, and Ag + PdNPs were obtained (Figure 6a) to analyze the optical properties of the nanoparticles precisely. As expected from the solution colors, the AgNPs exhibited a strong plasmon absorption band at 405 nm, whereas the UV−vis spectra of the PdNPs, Au + PdNPs, and Ag + PdNPs were almost flat. We also observed the structures of the synthesized AgNPs, PdNPs, Au + PdNPs, and Ag + PdNPs using TEM (Figure 6b). The four types of nanoparticles were mainly quasi-spherical and 20, 5, 10, and 10 nm in diameter. We analyzed the elemental composition of the Au + Pd and Ag + PdNPs using energy-dispersive X-ray spectroscopy (EDS) (Figure S2, Supporting Information). The atomic proportions of the two elements (Au and Pd of Au + PdNPs and Ag and Pd of Ag + PdNPs) in each bimetallic nanoparticle were both almost 1:1, owing to the similar reduction potential of the metal precursors (E° of $AuCl_4^-$ = 1.002 V; E° of Pd^{2+} = 0.951 V; E° of Ag^+ = 0.7996 V).[31]

After synthesizing pAAm-AuNPs with 10× $HAuCl_4$ and 1× SC, we investigated their stability against high ionic strength using NaCl. We conclude that pAAm-AuNPs were stabilized by pAAm and SC, following the synthetic mechanism discussed in Figure 2. To examine how strongly the surface ligands protect the pAAm-AuNPs, we incubated the pAAm-AuNPs with high salt concentrations (1, 2, and 2.5 M NaCl). Even after three days, the UV−vis spectra and solution colors of the pAAm-AuNPs did not change (Figure 7a), indicating excellent colloidal stability of the pAAm-AuNPs against high

https://doi.org/10.1021/acsomega.2c05813
ACS Omega 2022, 7, 45277−45286

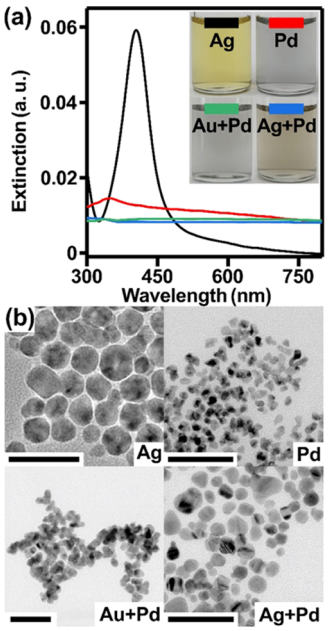

Figure 6. (a) UV−vis spectra of the AgNPs, PdNPs, and Au + Pd and Ag + Pd bimetallic nanoparticles (Au + PdNPs and Ag + PdNPs) synthesized in a mixture of EG and AAm. Photographs of the AgNP, PdNP, Au + PdNP, and Ag + PdNP solutions are shown in the inset. (b) TEM images of the AgNPs, PdNPs, Au + PdNPs, and Ag + PdNPs. All scale bars are 50 nm.

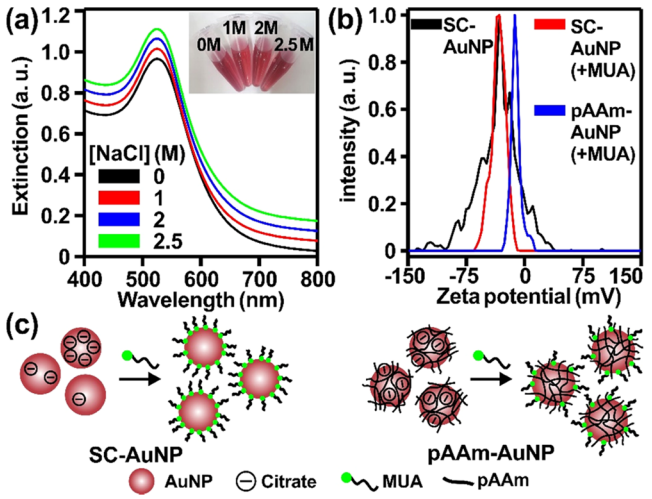

Figure 7. (a) UV−vis spectra of the pAAm-AuNPs incubated with NaCl at various concentrations (0, 1, 2, and 2.5 M) for 3 days. The UV−vis spectra were completely overlapped owing to the stability of the pAAm-AuNPs. For easier identification, the spectra of the pAAm-AuNPs after incubation with 1, 2, and 2.5 M of NaCl were intentionally shifted by increasing an extinction as much as 0.05, 0.1, and 0.15, respectively. A photograph of the pAAm-AuNP solutions is shown in the inset. (b) ζ-potential measurement of the as-synthesized SC-AuNPs and the SC-AuNPs and pAAm-AuNPs after incubation with 11-mercaptoundecanoic acid (MUA). (c) Schematic illustrations depicting the SC-AuNPs and pAAm-AuNPs before and after incubation with MUA.

ionic strength. In addition, the stability of the pAAm-AuNPs in biological media was also investigated by the incubation in phosphate buffer saline (0.8×), and minimum essential medium (0.8×) at room temperature. Even after 3 days, the UV−vis spectra and solution colors of the pAAm-AuNPs did not change, indicative of the high stability of the pAAm-AuNPs in biological media (Figure S3, Supporting Information). This stability implies strong binding of pAAm to the surface of AuNPs, which was examined using 11-mercaptoundecanoic acid (MUA). MUA is known for its high binding affinity to AuNPs owing to the thiol group.[32] We examined how strongly pAAm was bound to the surface of the pAAm-AuNPs by monitoring the zeta potential of the SC-AuNPs and pAAm-AuNPs after their incubation with MUA. In Figure 7b, the SC-AuNPs, after incubation with MUA, still exhibited a strong negative charge (−36.9 mV) and showed a sharper and more distinct zeta-potential distribution than that of the SC-AuNPs, indicating that unevenly distributed SC ligands on the SC-AuNPs were thoroughly exchanged with MUA. The surface charge of pAAm-AuNPs after incubation with MUA became more negative (−12.6 mV) than that before incubation with MUA (−7.5 mV) (Figure 2g). This minor change indicates that the pAAm ligands seemed to be rarely exchanged with MUA and that only a small amount of SC on the pAAm-AuNP surface was exchanged with MUA (Figure 7c). This result demonstrates that pAAm has a higher binding affinity than the thiol group, possibly because of the polymeric nature of pAAm. We further prepared a proposed synthesis mechanism in consideration of the size, stability, and surface charge of the pAAm-AuNPs in association with the polymerization of AAm in Scheme 2.

Scheme 2. Proposed Synthesis Mechanism of the pAAm-AuNPs

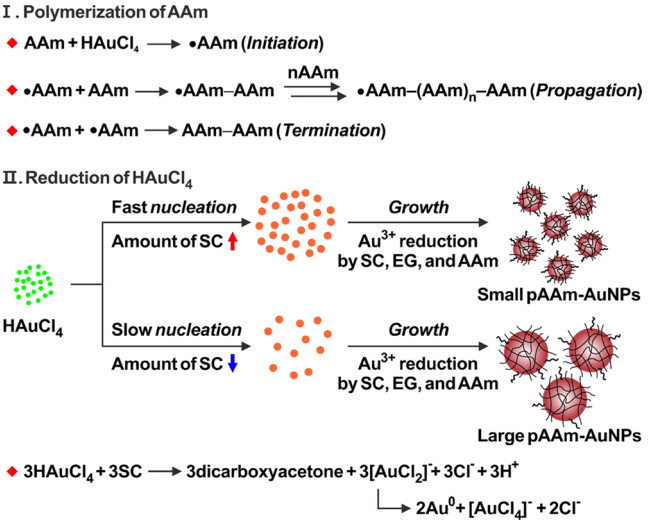

The catalytic activity of the pAAm-AuNPs was evaluated for the reduction of 4-nitrophenol to 4-aminophenol. This catalytic reaction is not only valuable for the removal of pollutant 4-nitrophenol but it also plays a role as an indicator to demonstrate the status of the surface protection and exposure. As expected, the absorption band (λ_{max} = 400 nm) of 4-nitrophenol was observed to shift from 400 to 300 nm with the color change from yellow to colorless, indicative of its catalytic reduction to 4-aminophenol owing to the catalytic surface of the pAAm-AuNPs (Figure 8a). This reaction was similarly observed with the SC-AuNPs. As the AuNPs were repeatedly reused as catalysts for the same reaction with newly prepared 4-nitrophenol solutions; however, the catalytic properties of the two types of AuNPs differed significantly.

https://doi.org/10.1021/acsomega.2c05813
ACS Omega 2022, 7, 45277−45286

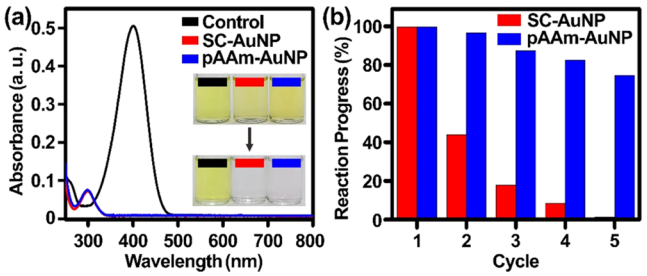

Figure 8. (a) UV−vis spectra of 4-nitrophenol solutions before and after the catalytic reduction using the SC-AuNPs and pAAm-AuNPs. The distinctive absorption band of 4-nitrophenol at 400 nm shifted to 300 nm after the reaction, indicative of its successful catalytic reduction to 4-aminophenol. The solution color changes are shown in the inset. (b) Reaction progress of each catalytic reduction cycle using the repeatedly used SC-AuNPs and pAAm-AuNPs as catalysts. The reaction progress was measured using the absorbance changes at 400 nm for five cycles.

The reduction of 4-nitrophenol was almost complete with the fresh SC-AuNPs, which almost did not occur with the SC-AuNPs that were repeatedly used five times (Figure 8b). The UV−vis spectra of the 4-nitrophenol solutions after each catalytic reduction cycle are shown in Figure S4 (Supporting Information). This deactivation was caused by the irreversible aggregation of the SC-AuNPs under highly reductive and high ionic strength conditions and, consequently, the decreased surface area. Unlike the insufficiently protected SC-AuNPs, however, the pAAm-AuNPs exhibited excellent catalytic activity until the fifth cycle, with a decrease of the reaction progress to 75%. The chemical stability of the pAAm-AuNPs is attributed to the sufficient protection of their surfaces by pAAm, whose presence was proved by the FT-IR spectra (Figure 2f). Considering that balancing the surface coverage for protection and the surface exposure for catalysis is an ongoing issue with heterogeneous catalysts, particularly nanoparticles, our approach to synthesize the pAAm-AuNPs could be a solution to address this concern.

The synthetic method presented in this study includes polymerization of the solvent and its concomitant viscosity controlled by EG during the synthesis. We recently reported that such solvent polymerization could stabilize highly concentrated AuNPs during their synthesis, increasing the possibility of achieving a gram-scale synthesis of the AuNPs using the method presented in this study.[9] For the gram-scale synthesis of the pAAm-AuNPs, the reaction scale was increased over 30 times. The UV−vis spectrum of the as-synthesized pAAm-AuNPs (Figure 9a) was very similar to that of AuNPs synthesized in a small batch (Figure 4), indicating their similar structural and optical properties. Moreover, the lyophilized pAAm-AuNP dry powder readily dissolved in water, and its UV−vis spectrum was similar to that of the as-synthesized pAAm-AuNPs. As expected from the UV−vis spectrum, TEM analysis revealed that the diameter of the spherical AuNPs was approximately 20 nm (Figure 9b), similar to that of the AuNPs obtained from the small-batch synthesis (Figure 4). Importantly, the final mass of the AuNPs produced from a single large-batch synthesis was 1.4734 g (yield: > 94%), with reaction volume and time of 91.5 mL and 5 min, respectively (Figure 9c). According to the concept of productivity that describes the efficiency of the synthesis considering the mass of the synthesized AuNPs per given synthesis reaction volume during a given reaction time in g h^{-1} L^{-1}, the gram-scale

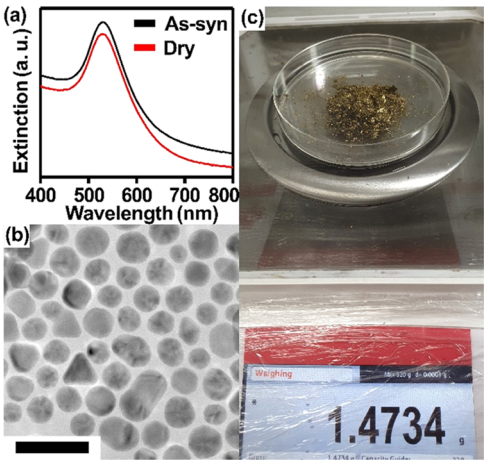

Figure 9. (a) UV−vis spectra of the as-synthesized pAAm-AuNPs (as-syn) and dissolved pAAm-AuNPs after lyophilization (dry). The two UV−vis spectra were almost overlapped and were intentionally shifted along the *y*-axis (extinction) for easier identification. (b) TEM image of the pAAm-AuNPs synthesized in gram scale. The scale bar is 50 nm. (c) Photograph showing the dry pAAm-AuNP powder and its mass (1.4734 g) from an electronic balance.

synthesis in this study is the most efficient (productivity = 193.23 g h^{-1} L^{-1}) among the gram-scale AuNP synthesis methods reported to date (Table S2, Supporting Information).[1−10]

CONCLUSIONS

We developed a new method of solution-based gram-scale synthesis of nanoparticles using liquefied AAm as a solvent. Despite its carcinogenicity and flammability, AAm was chosen because of its unique properties, such as a low melting temperature, high solvating power for metal precursors and reductants, and high miscibility in water for its removal. In addition, the exothermic polymerization of AAm resulted in the rapid synthesis of the nanoparticles in 5 min. Importantly, this study is the first to demonstrate an acrylic monomer as a solvent for synthesizing noble metal (Au, Ag, Pd, Ag + Pd, and Au + Pd) nanoparticles, unlike previous studies in which nanoparticles were synthesized with aqueous acrylic monomers for surface protection or within acrylic-based hydrogels for post-synthetic immobilization.[33,34] We further developed a method to control the viscosity of the AAm solvent by its polymerization and diluent addition, crucial for the gram-scale synthesis of the AuNPs with, to the best of our knowledge, the highest productivity. This approach could potentially be extended to the gram-scale synthesis of anisotropic nanoparticles using shape-directing agents in the initial mixture. Moreover, more polymerizable solvent systems need to be developed using new monomers and applicable reactions, such as condensation, ring-opening, and free radical/cationic/anionic addition, for the gram-scale synthesis of nanoparticles.

ASSOCIATED CONTENT

Supporting Information

The Supporting Information is available free of charge at https://pubs.acs.org/doi/10.1021/acsomega.2c05813.

Diameter distribution of Au nanoparticles; energy-dispersive X-ray spectra; UV−vis spectra of Au nanoparticles in various media; catalytic properties of Au nanoparticles; atomic proportion of the bimetallic (Au +

https://doi.org/10.1021/acsomega.2c05813
ACS Omega 2022, 7, 45277−45286

Pd and Ag + Pd) nanoparticles; summary of the amount of metal precursors used for the synthesis of Ag, Pd, Au + Pd, and Ag + Pd nanoparticles; summary of previous gram-scale synthesis studies of Au nanoparticles (PDF)

AUTHOR INFORMATION

Corresponding Author

Jae-Seung Lee − *Department of Materials Science and Engineering, Korea University, Seoul 02841, Republic of Korea*; orcid.org/0000-0002-4077-2043; Email: jslee79@korea.ac.kr

Author

Yoon Hyuck Kim − *Department of Materials Science and Engineering, Korea University, Seoul 02841, Republic of Korea*

Complete contact information is available at: https://pubs.acs.org/10.1021/acsomega.2c05813

Notes

The authors declare no competing financial interest.

ACKNOWLEDGMENTS

This work was supported by the BK21 FOUR Program and the Basic Science Research Program through the National Research Foundation of Korea (NRF), which is funded by the Ministry of Education (4199990514635), and by an NRF grant funded by the Ministry of Science and ICT (NRF-2016R1A5A1010148 and NRF-2021R1A2C1012917). The TEM and SEM images were obtained at the Seoul Center of the Korea Basic Science Institute (KBSI, Republic of Korea). Gel permeation chromatograms were obtained at the Korea Polymer Testing and Research Institute (KOPTRI, Republic of Korea).

REFERENCES

(1) Stoeva, S.; Klabunde, K. J.; Sorensen, C. M.; Dragieva, I. Gram-scale synthesis of monodisperse gold colloids by the solvated metal atom dispersion method and digestive ripening and their organization into two-and three-dimensional structures. *J. Am. Chem. Soc.* **2002**, *124*, 2305−2311.

(2) Jana, N. R.; Peng, X. Single-phase and gram-scale routes toward nearly monodisperse Au and other noble metal nanocrystals. *J. Am. Chem. Soc.* **2003**, *125*, 14280−14281.

(3) Zheng, N.; Fan, J.; Stucky, G. D. One-step one-phase synthesis of monodisperse noble-metallic nanoparticles and their colloidal crystals. *J. Am. Chem. Soc.* **2006**, *128*, 6550−6551.

(4) Lohse, S. E.; Eller, J. R.; Sivapalan, S. T.; Plews, M. R.; Murphy, C. J. A simple millifluidic benchtop reactor system for the high-throughput synthesis and functionalization of gold nanoparticles with different sizes and shapes. *ACS Nano* **2013**, *7*, 4135−4150.

(5) Park, K.; Hsiao, M.-s.; Yi, Y.-J.; Izor, S.; Koerner, H.; Jawaid, A.; Vaia, R. A. Highly concentrated seed-mediated synthesis of monodispersed gold nanorods. *ACS Appl. Mater. Interfaces* **2017**, *9*, 26363−26371.

(6) Khanal, B. P.; Zubarev, E. R. Gram-Scale Synthesis of Isolated Monodisperse Gold Nanorods. *Chem. - Eur. J.* **2019**, *25*, 1595−1600.

(7) Bianchi, P.; Petit, G.; Monbaliu, J.-C. M. Scalable and robust photochemical flow process towards small spherical gold nanoparticles. *React. Chem. Eng.* **2020**, *5*, 1224−1236.

(8) Escudero, A.; González-García, L.; Strahl, R.; Kang, D. J.; Drzic, J.; Kraus, T. Large-Scale Synthesis of Hybrid Conductive Polymer−Gold Nanoparticles Using "Sacrificial" Weakly Binding Ligands for Printing Electronics. *Inorg. Chem.* **2021**, *60*, 17103−17113.

(9) Kim, Y. H.; Oh, J.-H.; Lee, J.-S. Solid−Solution−Solid (SSS) Phase Transitions for Gram-Scale and High-Throughput Synthesis of Noble Metal Nanoparticles in Deep Eutectic Solvents. *J. Ind. Eng. Chem.* **2022**, *112*, 182−192.

(10) Stoeva, S. I.; Smetana, A. B.; Sorensen, C. M.; Klabunde, K. J. Gram-scale synthesis of aqueous gold colloids stabilized by various ligands. *J. Colloid Interface Sci.* **2007**, *309*, 94−98.

(11) Kang, H.; Buchman, J. T.; Rodriguez, R. S.; Ring, H. L.; He, J.; Bantz, K. C.; Haynes, C. L. Stabilization of Silver and Gold Nanoparticles: Preservation and Improvement of Plasmonic Functionalities. *Chem. Rev.* **2019**, *119*, 664−699.

(12) Peng, L.; You, M.; Wu, C.; Han, D.; Öçsoy, I.; Chen, T.; Chen, Z.; Tan, W. Reversible phase transfer of nanoparticles based on photoswitchable host−guest chemistry. *ACS Nano* **2014**, *8*, 2555−2561.

(13) Reddy, K. P.; Meerakrishna, R.; Shanmugam, P.; Satpati, B.; Murugadoss, A. Rapid gram-scale synthesis of Au/chitosan nanoparticles catalysts using solid mortar grinding. *New J. Chem.* **2021**, *45*, 438−446.

(14) Unal, I. S.; Demirbas, A.; Onal, I.; Ildiz, N.; Ocsoy, I. One step preparation of stable gold nanoparticle using red cabbage extracts under UV light and its catalytic activity. *J. Photochem. Photobiol., B* **2020**, *204*, No. 111800.

(15) Bai, J.; Li, Y.; Du, J.; Wang, S.; Zheng, J.; Yang, Q.; Chen, X. One-pot synthesis of polyacrylamide-gold nanocomposite. *Mater. Chem. Phys.* **2007**, *106*, 412−415.

(16) Demirbas, A.; Büyükbezirci, K.; Celik, C.; Kislakci, E.; Karaagac, Z.; Gokturk, E.; Kati, A.; Cimen, B.; Yilmaz, V.; Ocsoy, I. Synthesis of long-term stable gold nanoparticles benefiting from red raspberry (Rubus idaeus), strawberry (Fragaria ananassa), and blackberry (Rubus fruticosus) extracts−gold ion complexation and investigation of reaction conditions. *ACS Omega* **2019**, *4*, 18637−18644.

(17) Magdeldin, S.; Enany, S.; Yoshida, Y.; Xu, B.; Zhang, Y.; Zureena, Z.; Lokamani, I.; Yaoita, E.; Yamamoto, T. Basics and recent advances of two dimensional-polyacrylamide gel electrophoresis. *Clin. Proteomics* **2014**, *11*, No. 16.

(18) Shaikh, S. M.; Hassan, M. K.; Nasser, M. S.; Sayadi, S.; Ayesh, A. I.; Vasagar, V. A comprehensive review on harvesting of microalgae using Polyacrylamide-Based Flocculants: Potentials and challenges. *Sep. Purif. Technol.* **2021**, *277*, No. 119508.

(19) Chen, M.; Wang, L.-Y.; Han, J.-T.; Zhang, J.-Y.; Li, Z.-Y.; Qian, D.-J. Preparation and study of polyacryamide-stabilized silver nanoparticles through a one-pot process. *J. Phys. Chem. B* **2006**, *110*, 11224−11231.

(20) Pardo-Yissar, V.; Gabai, R.; Shipway, A. N.; Bourenko, T.; Willner, I. Gold nanoparticle/hydrogel composites with solvent-switchable electronic properties. *Adv. Mater.* **2001**, *13*, 1320−1323.

(21) Frens, G. Controlled Nucleation for the Regulation of the Particle Size in Monodisperse Gold Suspensions. *Nat. Phys. Sci.* **1973**, *241*, 20−22.

(22) Singh, K. P.; Palmese, G. R. Enhancement of phenolic polymer properties by use of ethylene glycol as diluent. *J. Appl. Polym. Sci.* **2004**, *91*, 3096−3106.

(23) Kang, S. C.; Choi, Y. J.; Kim, H. Z.; Kyong, J. B.; Kim, D. K. Kinetics of acrylamide solution polymerization using potassium persulfate as an initiator byin situ IR. *Macromol. Res.* **2004**, *12*, 107−111.

(24) Kim, F.; Connor, S.; Song, H.; Kuykendall, T.; Yang, P. Platonic Gold Nanocrystals. *Angew. Chem., Int. Ed.* **2004**, *43*, 3673−3677.

(25) Bastús, N. G.; Merkoçi, F.; Piella, J.; Puntes, V. Synthesis of highly monodisperse citrate-stabilized silver nanoparticles of up to 200 nm: kinetic control and catalytic properties. *Chem. Mater.* **2014**, *26*, 2836−2846.

(26) Lu, X.; Mi, Y. Characterization of the interfacial interaction between polyacrylamide and silicon substrate by Fourier transform infrared spectroscopy. *Macromolecules* **2005**, *38*, 839−843.

(27) Feng, L.; Yang, H.; Dong, X.; Lei, H.; Chen, D. pH-sensitive polymeric particles as smart carriers for rebar inhibitors delivery in alkaline condition. *J. Appl. Polym. Sci.* **2018**, *135*, No. 45886.
(28) Delvecchio, F. C.; Brizuela, R. M.; Khan, S. R.; Byer, K.; Li, Z.; Zhong, P.; Preminger, G. M. Citrate and vitamin E blunt the shock wave-induced free radical surge in an in vitro cell culture model. *Urol. Res.* **2005**, *33*, 448−452.
(29) Ji, X.; Song, X.; Li, J.; Bai, Y.; Yang, W.; Peng, X. Size control of gold nanocrystals in citrate reduction: the third role of citrate. *J. Am. Chem. Soc.* **2007**, *129*, 13939−13948.
(30) Iqbal, M.; Usanase, G.; Oulmi, K.; Aberkane, F.; Bendaikha, T.; Fessi, H.; Zine, N.; Agusti, G.; Errachid, E.-S.; Elaissari, A. Preparation of gold nanoparticles and determination of their particles size via different methods. *Mater. Res. Bull.* **2016**, *79*, 97−104.
(31) Haynes, W. M. *CRC Handbook of Chemistry and Physics*; CRC Press, 2013.
(32) Katz, E.; Willner, I. Integrated nanoparticle−biomolecule hybrid systems: synthesis, properties, and applications. *Angew. Chem., Int. Ed.* **2004**, *43*, 6042−6108.
(33) Qiao, J.; Mu, X.; Qi, L. A versatile method for the preparation of poly-acrylamide derivative functionalized thermo-responsive gold nanoparticles. *J. Mater. Chem. B* **2013**, *1*, 5756−5761.
(34) Dolya, N.; Rojas, O.; Kosmella, S.; Tiersch, B.; Koetz, J.; Kudaibergenov, S. "One-Pot" In Situ Formation of Gold Nanoparticles within Poly (acrylamide) Hydrogels. *Macromol. Chem. Phys.* **2013**, *214*, 1114−1121.

https://doi.org/10.1021/acsomega.2c05813
ACS Omega 2022, 7, 45277−45286